Polarization Evolution in Strong Magnetic Fields

Jeremy S. Heyl

and

Nir J. Shaviv,
Theoretical Astrophysics, mail code 130-33, California Institute of Technology, Pasadena, CA 91125

ABSTRACT

Extremely strong magnetic fields change the vacuum index of refraction. Although this polarization dependent effect is small for typical neutron stars, it is large enough to decouple the polarization states of photons traveling within the field. The photon states evolve adiabatically and follow the changing magnetic field direction. The combination of a rotating magnetosphere and a frequency dependent state decoupling predicts polarization phase lags between different wave bands, if the emission process takes place well within the light cylinder. This QED effect may allow observations to distinguish between different pulsar emission mechanisms and to reconstruct the structure of the magnetosphere.

1. Introduction

Understanding the structure of the magnetic fields surrounding neutron stars may provide a key in developing models for the radio and X-ray emission from pulsars, pulsar spindown, soft-gamma repeaters and the generation of the magnetic fields themselves. Although the magnetic field is instrumental in models of many phenomena associated with neutron stars, measuring its structure over a range of radii is problematic. Observations of the thermal emission from the surface may constrain the magnetic field geometry near the star, and the slowing of the pulsar's rotation may yield an estimate of the strength of the field near the speed-of-light cylinder. Connecting these regimes is difficult.

The intense magnetic fields associated with neutron stars influence many physical processes – cooling (Heyl & Hernquist 1997c; Shibanov et al. 1995), atmospheric emission (Rajagopal, Romani & Miller 1997; Pavlov et al. 1994) and the insulation of the core (Heyl & Hernquist 1998b; Heyl & Hernquist 1998a; Schaaf 1990; Hernquist 1985). Even stronger fields such as thought to be found near AXPs and SGRs alter the propagation of light through the magnetosphere by way of quantum-electrodynamic (QED) processes and may further process the emergent radiation (Heyl & Hernquist 1997a; Heyl & Hernquist 1997b; Baring 1995; Baring & Harding 1995; Adler 1971), and distort our view of the neutron star surface (Shaviv, Heyl & Lithwick 1999).

Even for weaker fields, QED renders the vacuum anisotropic. The speed at which light travels through the vacuum depends on its direction, polarization and the local strength of the magnetic field. Although for neutron stars with $B < 10^{14}$ G this effect is too weak to grossly affect images and light curves of these objects, it is strong enough to decouple the propagating modes through the pulsar magnetosphere.

To lowest order in the ratio of the photon energy to the electron rest mass-energy, the index of refraction of a photon in a magnetic field is independent of frequency. Near the pair-production threshold, the photon propagation adiabatically merges with a postironium state (Shabad & Usov 1986). However, well above the pair-production threshold for weak fields ($m_e c^2 \ll E \ll m_e c^2 4.4\times10^{13}$ G$/B$) the low energy results again provide a good approximation (Tsai & Erber 1975) In the context of the field surrounding a neutron star, only photons with sufficiently high wavenumbers (the optical and blueward) will travel through a portion of the rapidly weakening magnetic field without their two polarization modes mixing.

At radio frequencies, the plasma surrounding the neutron star produces a similar effect (*e.g.* Cheng & Ruderman 1979, Barnard 1986). One would expect that radio emission will be initially polarized according to the direction of the local magnetic field. When one observes a pulsar at a particular instant, one sees emission from regions with various magnetic field directions; therefore, one would expect the polarization to cancel out substantially. However, one finds that pulsars exhibit a significant linear polarization. As the polarized radiation travels from its source, its polarization direction changes as the local magnetic field direction changes. At a distance from the star that is large when compared to its radius, the local magnetic field in the plane of the sky is parallel across the observed portion of the star. Since the field changes gradually, the polarization modes are decoupled, and the disparate linear polarizations can add coherently.

Previous authors have focussed on the propagation of polarized radio waves through the magnetosphere. At these frequencies, the vacuum polarization is safely neglected. Furthermore, they have assumed that the coupling of the two polarization modes occurs instantaneously. In this paper, we will treat the problem of vacuum polarization in particular and how the gradual coupling of the polarization modes affects the final polarization of the emergent radiation. At sufficiently high frequency the plasma only negligibly affects the radiation as it travels through the magnetosphere. The precise frequency at which the vacuum birefringence begins to dominate depends on the charge density of the magnetospheric plamsa. If we assume the Goldreich-Julian value (Goldreich & Julian 1969), we find that for

$$E_{\rm photon} > 0.035\,{\rm eV}\,\left(\frac{B}{10^{12}\ {\rm G}}\frac{P}{1\ {\rm sec}}\frac{n_{\rm GJ}}{n_e}\right)^{-1/2}, \tag{1}$$

the vacuum contribution to the birefringence dominates that of the plasma (the modes collapse where equality obtains (Mészáros 1992)). Our study of the vacuum-dominated regime, the optical and blueward, complements the work of Cheng & Ruderman (1979) and Barnard (1986) and will help to interpret observations of high-energy polarized radiation from neutron stars.

2. Small Amplitude Waves in the QED Vacuum

Kubo & Nagata (1981) (also Kubo & Nagata 1983) derive the equation of motion of polarization direciton on the Poincaré sphere as light travels through an inhomogeneous birefringent medium. Since their results assume that the medium is polarized but not magnetized, we first extend their results to include magnetization. The general equations derived describe how polarized radiation travels through any birefringent medium in the limit of geometric optics. We then focus on the propagation of high frequency radiation through pulsar magnetospheres and how measurements of the polarization of this radiation can constrain both the structure of the magnetic field and the emission process of the radiation. This extended formalism is more than adequate to also describe the plasma induced birefringence of radio waves. This could be used to extend the works of Cheng & Ruderman (1979) and Barnard (1986).

Kubo & Nagata (1983) find that the evolution of the polarization of a wave traveling through a birefringent and dichroic medium in the limit of geometric optics is given by

$$\frac{\partial \mathbf{s}}{\partial x_3} = \hat{\mathbf{\Omega}} \times \mathbf{s} + \left(\hat{\mathbf{T}} \times \mathbf{s} \right) \times \mathbf{s}, \tag{2}$$

where x_3 is the direction of propagation, $\mathbf{s}$ is the normalized Stokes vector (Jackson 1975), and $\hat{\mathbf{\Omega}}$ and $\hat{\mathbf{T}}$ are the birefringent and dichroic vectors. The Stokes vector consists of the four Stokes parameters, S_0, S_1, S_2 and S_3. The vector $\mathbf{s}$ consists of $S_1/S_0, S_2/S_0$ and S_3/S_0.

Waves traveling through a magnetized (or electrified) vacuum are best treated by linearizing the constitutive relations about the external field. Heyl & Hernquist (1997b) find that the permeability and dielectric tensors consist of an isotropic component plus an added component along the direction of the external field. Using the dielectric and permeability tensors of a magnetized vacuum in the formalism of Kubo & Nagata (1983) yields

$$\hat{\mathbf{\Omega}} = \frac{k_0}{2\sqrt{\mu_i \varepsilon_i + 1/2 \left(\mu_i \varepsilon_f + \mu_f \varepsilon_i \right) \sin^2 \theta}} \left(\mu_i \varepsilon_f - \mu_f \varepsilon_i \right) \sin^2 \theta \begin{bmatrix} \cos 2\phi \\ -\sin 2\phi \\ 0 \end{bmatrix}. \tag{3}$$

where θ is the angle between the direction of propagation ($\mathbf{k}$) and the external field and ϕ is the angle between the component of the external field perpendicular to $\mathbf{k}$ and the $x-$axis defined by the observer. μ_i and μ_f are the isotropic and along the field components of the permeability tensor. ε_i and ε_f are the equivalent dielectric tensors.

For the case of vacuum QED with an external magnetic field to one loop, we find that the amplitude of $\hat{\mathbf{\Omega}}$ is proportional to the difference between the indices of refraction for the two polarization states:

$$\Omega/k_0 = \Delta n = n_\perp - n_\parallel \tag{4}$$

$$= \frac{\alpha}{4\pi} \sin^2 \theta \left[-X_0^{(2)} \left(\frac{1}{\xi} \right) \xi^{-2} + X_0^{(1)} \left(\frac{1}{\xi} \right) \xi^{-1} - X_1 \left(\frac{1}{\xi} \right) \right] \tag{5}$$

to lowest order in α, the fine-structure constant. $\xi = B/B_{\rm QED}$ ($B_{\rm QED} \approx 4.4 \times 10^{13}$ G) and the functions $X_0(x)$ and $X_1(x)$ are defined in Heyl & Hernquist (1997a). An external electric field yields similar results. However, in this case the vacuum is also dichroic so the vector $\hat{\mathbf{T}}$ is nonzero.

In the weak magnetic field limit ($\xi \ll 0.5$) we obtain,

$$n_\perp - n_\parallel = \frac{\alpha}{4\pi}\frac{2}{15}\xi^2 \sin^2\theta, \tag{6}$$

and the strong field limit ($\xi \gg 0.5$) yields

$$n_\perp - n_\parallel = \frac{\alpha}{4\pi}\frac{2}{3}\xi \sin^2\theta. \tag{7}$$

2.1. Exact Solutions

Kubo & Nagata (1983) found that Equation 2 yields exact solutions for restricted values of $\hat{\mathbf{\Omega}}$ and $\hat{\mathbf{T}}$. In the case of a uniformly magnetized vacuum, $\hat{\mathbf{T}} = 0$ and $\hat{\mathbf{\Omega}}$ is constant. In this case, the polarization vector $\mathbf{s}$ traces a circle on the Poincaré sphere about the vector $\hat{\mathbf{\Omega}}$ at a rate of $|\hat{\mathbf{\Omega}}|$.

Kubo & Nagata (1981) examine the case where $\hat{\mathbf{\Omega}}$ is constant in magnitude but satisfies,

$$\frac{\partial \hat{\mathbf{\Omega}}}{\partial x_3} = \mathbf{\Upsilon} \times \hat{\mathbf{\Omega}} \tag{8}$$

where $\mathbf{\Upsilon}$ is a constant. In this case $\hat{\mathbf{\Omega}}$ rotates about $\mathbf{\Upsilon}$ at a rate of $|\mathbf{\Upsilon}|$. If we follow the equations in a rotating coordinate system such that in it $\hat{\mathbf{\Omega}}'$ is constant, we find that $\mathbf{s}'$ satifies the following equation

$$\frac{\partial \mathbf{s}'}{\partial x_3} = \hat{\mathbf{\Omega}}_{\rm eff} \times \mathbf{s}' \tag{9}$$

where

$$\hat{\mathbf{\Omega}}'_{\rm eff} = \hat{\mathbf{\Omega}}' - \mathbf{\Upsilon}. \tag{10}$$

This equation holds even if $\mathbf{\Upsilon}$ is not constant. However, if $\mathbf{\Upsilon}$ is constant, we obtain a new exact solution where $\mathbf{s}$ circles a guiding center displaced from $\hat{\mathbf{\Omega}}$ which in turn rotates about $\mathbf{\Upsilon}$.

If we take $\mathbf{s} \parallel \hat{\mathbf{\Omega}}$ initially and $\mathbf{\Upsilon} \perp \hat{\mathbf{\Omega}}$, we find that $\mathbf{s}$ develops a component perpendicular to $\hat{\mathbf{\Omega}}$. In the case of vacuum QED, $\hat{\mathbf{\Omega}}$ lies in the $1-2-$plane. If the magnetic field rotates uniformly in the plane transverse to the wave, we find that $\mathbf{s}$ will leave the $1-2-$plane and a circularly polarized component will develop.

2.2. Adiabatic Approximation

If the parameters describing the motion of a system vary slowly compared to the characteristic frequency of the system, the system evolves adiabatically such that at a given time it executes a

motion given by the instantaneous values of the parameters as if they were static. The exact solution given by Equation 9 has this feature if $|\hat{\mathbf{\Omega}}| \gg |\mathbf{\Upsilon}|$. If this limit applies, $\hat{\mathbf{\Omega}}_{\rm eff}$ is nearly parallel to $\hat{\mathbf{\Omega}}'$ and $\mathbf{s}$ circles the instantaneous guiding center $\hat{\mathbf{\Omega}}$. Furthermore, if $\mathbf{s}$ is initially parallel or antiparallel to $\hat{\mathbf{\Omega}}$, it will remain so (corresponding to polarizations that are parallel or perpendicular to the direction of the magnetic field). That is, the polarization modes are decoupled, and the polarization direction follows the direction of the magnetic field.

We can also build an adiabatic approximation onto the exact solution of Equation 9 by allowing the magnitude of $\hat{\mathbf{\Omega}}$ to vary. We take a wave polarized parallel to the initial value of $\hat{\mathbf{\Omega}}$. As $\hat{\mathbf{\Omega}}$ rotates about Υ and decreases in magnitude, $\mathbf{s}$ rotates about $\hat{\mathbf{\Omega}}_{\rm eff}$ and follows the instantaneous direction of $\hat{\mathbf{\Omega}}_{\rm eff}$ as long as

$$\left| \hat{\mathbf{\Omega}} \left(\frac{1}{|\hat{\mathbf{\Omega}}|} \frac{\partial |\hat{\mathbf{\Omega}}|}{\partial x_3} \right)^{-1} \right| \gg 1. \tag{11}$$

Numerical integration of Equation 2 for $|\hat{\mathbf{\Omega}}| = A x_3^{-6}$ and $\mathbf{\Upsilon} = -1/10 \hat{x}_3$ ($\hat{\mathbf{\Omega}}$ rotates by one radian after the photon has travelled 10 units of distance) shows that the polarization follows the analytic solution described in the previous paragraph for

$$\left| \hat{\mathbf{\Omega}} \left(\frac{1}{|\hat{\mathbf{\Omega}}|} \frac{\partial |\hat{\mathbf{\Omega}}|}{\partial x_3} \right)^{-1} \right| \gtrsim 0.5 \tag{12}$$

and then freezes for values of A ranging from 10 to 10^8. Figure 1 depicts both the numerical results and the analytic approximation.

Generically, if the polarization modes of the medium are linear, and the wave begins in one of the modes, the final direction of the polarization projected into the $S_1 - S_2-$plane will depend on *how much* the field direction has changed by the time of mode coupling. The circular component of the polarization depends on *how fast* the field direction is changing at the time of mode coupling.

By applying these results to a magnetic dipole in vacua, we find that an outgoing photon's polarization will follow the analytic solution until

$$\frac{3}{2} \frac{{\rm d} \ln \Delta n}{{\rm d} \ln B} \frac{B^{1/3}}{\Delta n} = k_0 R_0 B_0^{1/3}, \tag{13}$$

after which its polarization in the observer's system freezes. The left side of the equality describes the environment at the point when the polarization freezes; the right side depends on the point of emission of the photon. Figure 2 shows the magnetic field strength at coupling as a function of photon energy for typical pulsar parameters.

If the modes begin to mix where $B \ll B_{\rm QED}$ (this is appropriate for all but the lowest energy photons near the most strongly magnetized neutron stars), we obtain

$$\frac{B_{\rm couple}}{B_0} = \left[\frac{\alpha}{4\pi} \frac{2}{45} \left(\frac{B_0}{B_{\rm QED}} \right)^2 k_0 R_0 \right]^{-5/3} \tag{14}$$

$$= \quad 1.95 \times 10^{-5} \left(\frac{E}{1 \text{ eV}}\right)^{-5/3} \left(\frac{B_0}{10^{12} \text{ G}}\right)^{-10/3} \left(\frac{R_0}{10^6 \text{ cm}}\right)^{-5/3}. \tag{15}$$

If this ratio is less than unity for a photon, the photon will travel with its polarization modes decoupled during some portion of its journey away from the star. That is, if

$$E > 1.49 \times 10^{-3} \text{ eV} \left(\frac{B_0}{10^{12} \text{ G}}\right)^{-2} \left(\frac{R_0}{10^6 \text{ cm}}\right)^{-1}, \tag{16}$$

the vacuum will decouple the polarization modes. For parameters typical to neutron stars, the polarization modes for all photons with $\lambda \lesssim 800$ μm will be decoupled at least as they begin their journey from the vicinity of the neutron star. Although for photons of such low energy, the mode coupling induced by the plasma is likely to dominate (*e.g.* Cheng & Ruderman 1979).

These effects may also be important for photons travelling through the magnetospheres of strongly magnetized white dwarfs. The most strongly magnetized white dwarfs have $B \sim 10^9$ G and $R_0 \sim 10^9$ cm; in the magnetospheres of these stars, the polarization modes of photons more energetic than 1.5 eV will be decoupled by the vacuum birefringence.

3. Rotating Pulsar Magnetospheres

The photons that we observe from neutron stars have to travel through a portion of the neutron star's magnetosphere before reaching us. If they travel through a region where Equation 11 holds, the photon's polarization relative the observer's axes will change as the magnetic field direction changes. If we examine a photon which leaves the surface of the star, once it has travelled a distance of several radii it will be travelling approximately radially. If the magnetic moment of the star remains fixed during the journey and the modes remained decoupled, the polarization directions of all the photons travelling in a particular direction and polarization mode will align with each other.

The plasma in the vicinity of a neutron star is polarized by passing waves of sufficiently low frequencies. Cheng & Ruderman (1979) used this effect to explain the high linear polarization of radio emission from pulsars even though one would expect the polarization modes where the radiation is produced to vary from place to place. The same effect will operate at high frequencies through the vacuum polarization of QED.

High frequency photons travelling through a pulsar magnetosphere may travel a large distance before the modes couple. During this travel, the magnetic field of the pulsar may rotate a significant amount, thereby changing the polarization modes in the observer's frame as the photon travels. Since high energy photons travel further than less energetic ones, the higher energy photons will have their polarizations dragged further by the rotating magnetic field.

3.1. Analytic Treatment

If we assume that the rotation rate of the projection of the magnetic field onto the plane transverse to a photon's propagation changes sufficiently slowly, we can apply the results of § 2.2 to calculate the final polarization of the photon. What is required is the direction of magnetic field at the point of recoupling and its rate of change.

This analytic treatment will be restricted to photons travelling in the radial direction. For a significant phase lag to develop, the polarization modes must remain decoupled until well away from the star. Here outgoing photons emitted from near the stellar surface will have approximately radial trajectories. Furthermore, at these distances both gravitational light bending and magnetic lensing (Shaviv, Heyl & Lithwick 1999) may be neglected.

The photon's trajectory will be characterized by the angles ξ and θ the longitude and colatitude where the photon left the star. We shall take ϖ, the phase of the star's rotation, to be zero when the photon leaves the surface. The magnetic pole lies at zero longitude and colatitude Ψ. As the photon travels away from the neutron star, the phase ϖ increases and the local magnetic field direction changes. The criterion for recoupling in the weak-field limit when travelling through a dipole field is

$$\frac{2}{15}\frac{\alpha}{4\pi}\left(\frac{B_{0,\mathrm{equator}}}{B_{\mathrm{QED}}}\right)^2 R_0^6 k_0 \frac{\sin^2\alpha}{r^6}\left|\frac{\mathrm{d}\sin^2\alpha}{\mathrm{d}r}\frac{1}{\sin^2\alpha}-\frac{6}{r}\right|^{-1}=\frac{1}{2} \tag{17}$$

In this equation, the angle α designates the magnetic colatitude of the photon which changes as the star rotates underneath it. It satisfies the following expression

$$\cos\alpha = \sin\theta\cos(\xi+\varpi)\sin\Psi+\cos\Psi\cos\theta. \tag{18}$$

The second important angle is the angle between the observer's axes and the local magnetic field direction in the plane of the sky. For a magnetic dipole, the projection of the local magnetic direction and the projection of the magnetic moment ($\hat{\mathbf{m}}$) onto the tangential plane are colinear. Unless the line of sight is directed down the rotation axis, we can use the projection of the rotation axis ($\hat{\mathbf{z}}$) as one of the reference axes for measuring the polarization of the radiation. These projected vectors are defined by

$$\mathbf{z}_{\mathrm{p}} = \hat{\mathbf{z}}-\hat{\mathbf{r}}\cos\theta \tag{19}$$

$$\mathbf{m}_{\mathrm{p}} = \hat{\mathbf{m}}-\hat{\mathbf{r}}\cos\alpha. \tag{20}$$

The travelling photon does not distinguish between a magnetic field pointing in one direction or in the exactly opposite direction (see Equation 3); therefore, we only need to know the angle between $\mathbf{z}_{\mathrm{p}}$ and $\mathbf{m}_{\mathrm{p}}$ modulo π. Calculating the cross product suffices to give the magnitude of the angle,

$$(\mathbf{z}_{\mathrm{p}}\times\mathbf{m}_{\mathrm{p}})\cdot\hat{\mathbf{r}} = z_{\mathrm{p}} m_{\mathrm{p}}\sin\phi, \tag{21}$$

which yields

$$\tan\phi = \frac{\sin(\xi+\varpi)}{\cos\theta\cos(\xi+\varpi)-\cot\Psi\sin\theta}. \tag{22}$$

$\boldsymbol{\Upsilon}$ in this case is given by

$$\boldsymbol{\Upsilon} = -2\frac{\mathrm{d}\phi}{\mathrm{d}\varpi}\frac{2\pi}{cP}\,\hat{3}. \tag{23}$$

So the final polarization of the photon in the observers frame is given by Equation 10 evaluated at the moment of recoupling.

The calculation of the polarization evolution in the analytic treatment proceeds as follows,

1. Choose the colatitude of the observer (θ), the longitude where the photon is emitted (ξ), a reference frequency and magnetic field strength.

2. Given the period of the pulsar (P), a photon's radius is given by

$$r = \frac{cP}{2\pi}\varpi + R_0. \tag{24}$$

   For a given value of ϖ, the phase, solve for $B^2_{0,\mathrm{equator}}k_0$ assuming that Equation 17 is satisfied, and calculate the magnitude of $\hat{\boldsymbol{\Omega}}$ at recoupling.

3. Substitute this value of ϖ into Equation 22 to calculate the direction of $\hat{\boldsymbol{\Omega}}$ at recoupling.

4. Finally, calculate $\boldsymbol{\Upsilon}$ at recoupling using Equation 23. The final polarization according to this analytic adiabatic approximation lies along

$$\hat{\boldsymbol{\Omega}}_{\mathrm{eff}} = \hat{\boldsymbol{\Omega}} - \boldsymbol{\Upsilon}. \tag{25}$$

5. This procedure can be repeated for other values of the longitude (ξ) to generate a light curve.

In the case where the line of sight is aligned with the rotation axis, many of these geometric considerations vanish, and the problem reduces identically to that treated in § 2.2.

In this situation we can derive expressions for both the final position angle,

$$\phi = \frac{2\pi}{cP}\left\{\frac{1}{90}\left[\alpha\frac{90^4}{\pi}k_0R_0^6\left(\sin\Psi\frac{B_{0,\mathrm{equator}}}{B_{\mathrm{QED}}}\right)^2\right]^{1/5} - R_0\right\} \tag{26}$$

$$\approx 7.7\times10^{-4}\left(\sin\Psi\frac{B_{0,\mathrm{equator}}}{10^{12}\ \mathrm{G}}\right)^{2/5}\left(\frac{E_{\mathrm{photon}}}{1\ \mathrm{eV}}\right)^{1/5}\left(\frac{P}{1\ \mathrm{sec}}\right)^{-1}\left(\frac{R_0}{10^6\ \mathrm{cm}}\right)^{6/5} \tag{27}$$

and the circular component,

$$s_3/|\mathbf{s}| = \frac{4\pi}{cP}\left[\left(\frac{3}{r}\right)^2 + \left(\frac{4\pi}{cP}\right)^2\right]^{-1/2}, \tag{28}$$

where

$$r = \phi\frac{cP}{2\pi} + R_0. \tag{29}$$

If $|s_3|/|\mathbf{s}| \ll 1$, the following approximation holds,

$$s_3/|\mathbf{s}| \approx \frac{2}{3}\phi + \frac{4}{3}\pi\frac{R_0}{cP}. \tag{30}$$

For a more general pulsar geometry we can still use Equation 26 to characterize how radiation at various frequencies is polarized. Specifically, the position angle can be converted to a time lead for the polarization angle of high-frequency relative to low-frequency radiation. This time lead given by $P\phi/(2\pi)$ is independent of the period of the pulsar. Figure 4 plots the known radio pulsars (Taylor, Manchester & Lyne 1993) and the approximate phase lead ($r_{\rm couple}/r_{\rm lc}$) expected at 5.2 keV relative to zero-energy photons. If $r_{\rm couple}$ is a large fraction of the radius of the light cylinder, it may be possible to study the geometry of the magnetic field at large distances from the pulsar. For the Crab pulsar the radius at coupling for 5.2 keV is about 16% of the light-cylinder radius. The millisecond pulsars, PSR J1939+2134 and PSR J1824-2452, have $r_{\rm couple}$ of over 9% of $r_{\rm lc}$ at 5.2 keV.

3.2. Numerical Treatment

The analytic techniques outlined in the previous subsection provide insights to interpret and extend the results from a direct numerical integration of Equation 2. Nevertheless, a numerical integration is unavoidable if we wish to calculate the phase shifts under general conditions – when the observer's inclination angle is nontrivial and the field is not strictly dipolar.

The numerical integration assumes two basic assumptions:

1. We assume that either
   (a) The magnetosphere is co-rotating with the NS. This implies that the local magnetic field is at any given moment aligned with the NS, irrespective of the distance. (A deviation from this behavior will indicate where the co-rotating magnetosphere ends), *or*
   (b) The magnetic field is given by that of a magnetized conducting sphere rotating *in vacua* (Deutsch 1955, Barnard 1986)
2. The photon is traveling radially. That is to say, the emission process takes place well within the region where the polarization states couple.

With these assumptions considered, the integration is achieved in a straightforward manner. A photon is followed from an initial radius R_0 to a radius $r_{\rm final}$ that is beyond the recoupling distance using the equation:

$$\frac{\partial \mathbf{s}}{\partial r} = \hat{\mathbf{\Omega}} \times \mathbf{s}. \tag{31}$$

Each radial step is integrated forward using the fourth order Runge-Kutta algorithm. To do so, one has to calculate the birefringent vector $\hat{\mathbf{\Omega}}$ using Equation 22 for the angle of the magnetic field and

Equation 6 for the strength of the birefringence. To calculate this vector for the Deutsch (1955) fields, we use Eq. 7 of Barnard (1986). The rotation phase of the star is related to the radial coordinate through Equation 24.

3.2.1. The Crab pulsar

The Crab pulsar is among the most thoroughly studied astronomical objects. Its fast period and moderately strong magnetic field make it an ideal example for this process. We take $\theta = 54^\circ$ and $\Psi = 64^\circ$ which reproduces the magnitude of the polarization swing for the pulse and interpulse (Smith et al. 1988), and the field strength at the magnetic equator to be 1.9×10^{12} G (Taylor, Manchester & Lyne 1993). The results of this calculation are depicted in Figure 5 and Figure 6. If the field is indeed a corotating dipole, the delayed coupling of the polarization modes results in the polarization of high frequency radiation leading that of lower energies. The lead time estimate from Equation 26 works well away from the pulse or interpulse where it slightly over or underestimates the lead time. However, if the neutron star is surrounded by a Deutsch field, this lead is retarded slightly.

Since the coupling of the modes occurs gradually, a significant circular component will develop when the modes are weakly coupled. If the radiation initially has a circular component, this initial component is washed out when one measures the circular polarization over a finite bandpass, leaving only the value of s_3 produced by the coupling. Both the Deutsch fields and the corotating dipole fields result in a significant amount of circular polarization (up to 30% of the total polarization for the corotating dipole at 5.2 keV or 7% of it at 4.5 eV). The circular polarization generated by the rotating Deutsch field peaks at about 65% of the total polarization at the highest frequency studied.

3.2.2. RX J0720.4-3125

RX J0720.4-3125 is an isolated neutron star candidate suspected to be close to the Earth. Heyl & Hernquist (1998c) from cooling arguments and its current period of 8.391 s estimate that it has a magnetic field of $B \sim 10^{14}$ G. From Equation 26 we estimate the time lead for a given frequency to be approximately five times larger than for the Crab pulsar. As we see from Figure 9, since the period of RX J0720.4-3125 is much larger than that of the Crab, the expected change in position angle over the larger lead time is very small. Furthermore, since the coupling of the modes occurs well within the light cylinder, the difference between the Deutsch and the corotating dipole model is negligible. Since the circular polarization that develops during coupling is proportional to the rotation frequency of the pulsar, very little circular polarization is evident in the emergent radiation – S_3 peaks at 2.7% of the total polarization, coincident with the pulse and interpulse.

4. Discussion

The vacuum polarization induced by quantum electrodynamics decouples the polarization modes in the strong magnetic field surrounding neutron stars. As radiation travels away from the neutron star, the modes of low-frequency radiation couple first; consequently, the position angle of low frequency emission will lag behind that of higher frequency radiation emitted coincidently and in the same mode. Puslars often exhibit mode switching as a function of phase and frequency. An inelegant way to avoid confusion is to examine the position angle modulo $\pi/2$. By measuring the position angle as a function of frequency, one can determine not only the location of the emission but also probe the structure of the magnetic field near the light cylinder using sufficiently high frequency radiation.

Previous authors have calculated a similar effect where the plasma decouples the modes at radio frequencies, assuming that the coupling occurs instantly (Cheng & Ruderman 1979; Barnard 1986). To relax this assumption, we use the equations describing the propagation of polarized radiation through a polarized and magnetized medium, under the assumptions of geometric optics. These results extend those of Kubo & Nagata (1981) to the case of a magnetized and polarized medium. Linearly polarized radiation will develop a circular component during the gradual coupling of the modes.

In the case of QED in a vacuum, the propagating modes are purely linear; therefore, the decoupling will wash out any initial circular component averaged over a finite bandpass. The only circular component present in the outgoing radiation is produced during coupling and measures the ratio of the coupling radius to the radius of the light cylinder. This circular component provides an independent validation of the effect.

Since high frequency radiation is generally measured incoherently, determining the Stokes parameters becomes more difficult with increasing photon energy. Blueward of the ultraviolet, measuring circular polarization is impractical. The Spectrum-X-Gamma mission will carry a stellar x-ray polarimeter (SXRP) which will be especially sensitive at 2.6 keV and 5.2 keV, the first and second-order Bragg reflections off of graphite. Future instruments may be able to measure both linear and circular polarization at yet higher energies.

From a theoretical point of view, the study of the propagating modes of a strongly magnetized vacuum is simpler than analysing those of a strongly magnetized plasma, especially when the properties of the plasma are not well known. However, given the magnetic permeability and the dielectric permittivity of the circumpulsar plasma, these results can be applied to study plasma-induced decoupling on the properties of polarized radio emission from pulsars. We leave the details of this process for a subsequent paper; however, our general arguments apply here as well.

Both the plasma-induced and vacuum-induced decoupling can be used to probe the structure of pulsar magnetospheres. A measurement of the circular polarization produced by the mode coupling yields an estimate of the radius of the coupling. The frequency corresponding to a given degree

of circular polarization measures the radial gradient of third power of the difference between the indices of refraction of the two modes. This results from the approximate inequality Equation 12. Like the arguments used in § 2.2, it is generic to waves travelling through a birefringent medium in the limit of geometric optics.

Unlike the phase lead effect found by previous authors for the case of the plasma alone, the circular polarization provides a local probe of the pulsar magnetosphere without having to compare observations over a wide range of energy. As long as the radiation is produced in a region where the modes are decoupled, the interpretation of the circular polarization is straightforward.

Measurements of the position angle of the radiation as a function of phase and frequency can also yield the same information, since the induced circular polarization is simply related to the phase lead. Furthermore, measuring all four Stokes parameters can elucidate the location of the emission process since below a critical frequency the modes will be coupled at the point of emission and the observed position angle will be constant with frequency. The circular polarization of the first modes which do travel through a decoupled region yields the radius of the emission. The details of the interpretation will only depend weakly on the medium which decouples the modes – plasma or vacuum.

We have derived equations which describe the propagation of polarized radiation through a magnetized and polarized medium. By applying these results to the strongly magnetized regions surrounding neutron stars, we have found several observational probes of pulsar magnetospheres and emission.

REFERENCES

Adler, S. L. 1971, *Ann. Phys.,* **67**, 599.

Baring, M. G. 1995, *ApJL,* **440**, 69.

Baring, M. G. & Harding, A. K. 1995, *Astrophys. Sp. Sci.,* **231**, 77.

Barnard, J. J. 1986, *ApJ,* **303**, 280.

Cheng, A. F. & Ruderman, M. A. 1979, *ApJ,* **229**, 348.

Deutsch, A. J. 1955, *Ann. d'Ap.,* **18**, 1.

Goldreich, P. & Julian, W. H. 1969, *ApJ,* **157**, 869.

Hernquist, L. 1985, *MNRAS,* **213**, 313.

Heyl, J. S. & Hernquist, L. 1997a, *Phys. Rev. D,* **55**, 2449.

Heyl, J. S. & Hernquist, L. 1997b, *Jour. Phys. A,* **30**, 6485.

Heyl, J. S. & Hernquist, L. 1997c, *ApJL,* **491**, 95.

Heyl, J. S. & Hernquist, L. 1998a, *MNRAS,* **300**, 599.

Heyl, J. S. & Hernquist, L. 1998b, *MNRAS,*, submitted

Heyl, J. S. & Hernquist, L. 1998c, *MNRAS,* **297**, L69.

Jackson, J. D. 1975, *Classical Electrodynamics*, John Wiley, New York, second edition

Kubo, H. & Nagata, R. 1981, *J. Opt. Soc. Am.,* **71**, 327.

Kubo, H. & Nagata, R. 1983, *J. Opt. Soc. Am.,* **73**, 1719.

Mészáros, P. 1992, *High-Energy Radiation from Magnetized Neutron Stars*, University of Chicago Press, Chicago

Pavlov, G. G., Shibanov, Y. A., Ventura, J. & Zavlin, V. E. 1994, *A&A,* **289**, 837.

Rajagopal, M., Romani, R. W. & Miller, M. C. 1997, *ApJ,* **479**, 347.

Schaaf, M. E. 1990, *A&A,* **227**, 61.

Shabad, A. E. & Usov, V. V. 1986, Ap&SS, **128**, 377.

Shaviv, N. J., Heyl, J. S. & Lithwick, Y. 1999, *MNRAS,* **306**, 333.

Shibanov, Y. A., Pavlov, G. G., Zavlin, V. E. & Tsuruta, S. 1995, in H. Böhringer, G. E. Morfill & J. E. Trümper (eds.), *Seventeenth Texas Symposium on Relativistic Astrophysics and Cosmology*, Vol. 759 of *Annals of the New York Academy of Sciences*, p. 291, The New York Academy of Sciences, New York

Smith, F. G., Jones, D. H. P., Dick, J. S. B. & Pike, C. D. 1988, *MNRAS,* **233**, 305.

Taylor, J. H., Manchester, R. N. & Lyne, A. G. 1993, *ApJS,* **88**, 529.

Tsai, W. Y. & Erber, T. 1975, *Phys. Rev. D,* **12**, 1132.

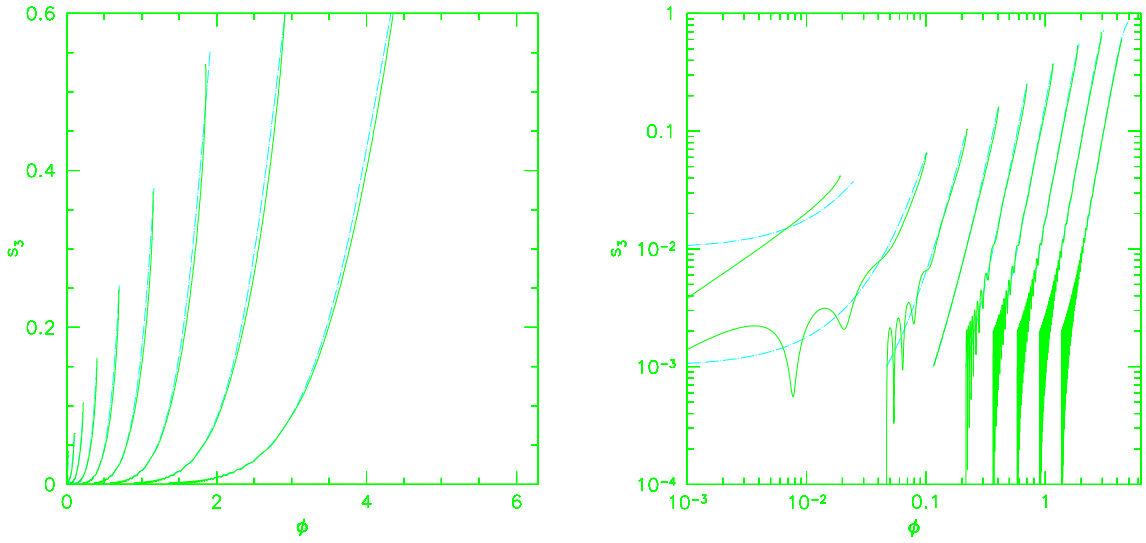

Fig. 1.— Numerical solution and analytic approximation. The figures depict the exact numerical solution (solid lines) and the analytic solution based on the adiabatic approximation (dashed lines).

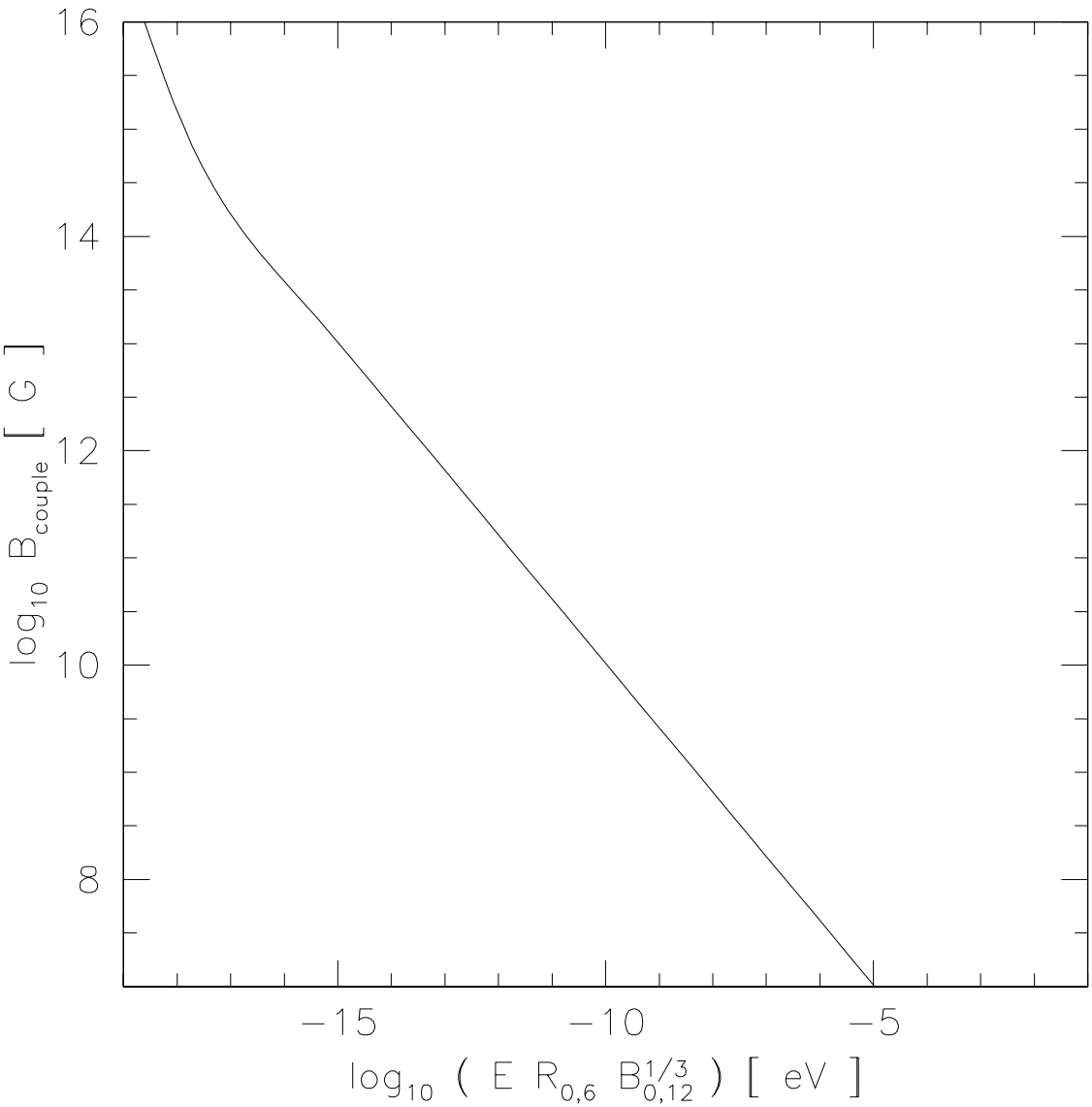

Fig. 2.— The dipole magnetic field strength at coupling. The strength of the magnetic field at coupling depends on the magnetic moment of the star and the energy of the photon. The modes of higher energy photons couple later (further from the star).

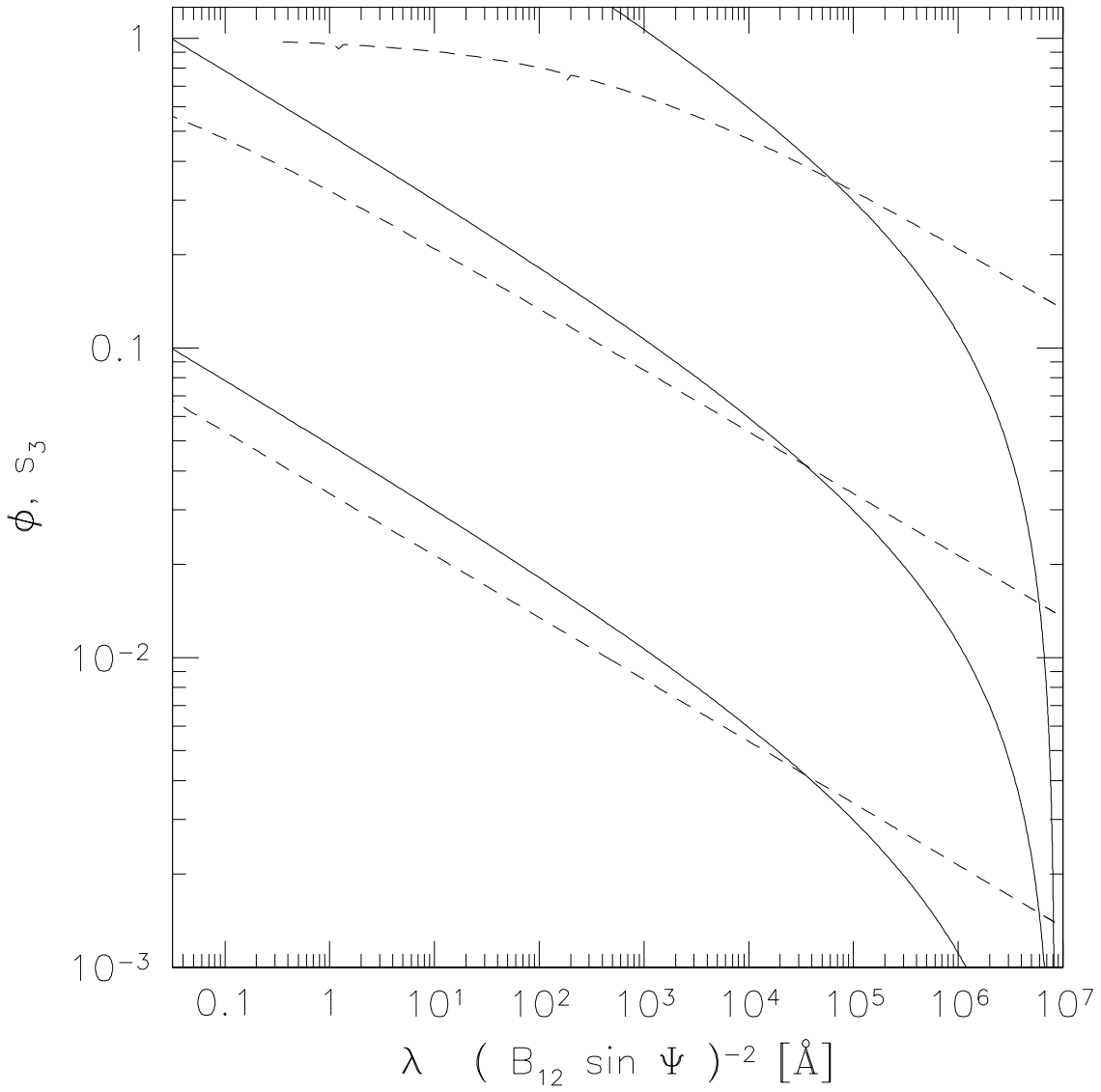

Fig. 3.— The observed polarization as a function of frequency for a line of sight parallel to the rotation axis in the presense of a rotating dipole field. The panel depicts the polarization angle (solid line) and circular component (dashed line, normalized to $|\mathbf{s}|$) as a function of wavelength. The lines from top to bottom trace the solutions for $P = 1, 10$, and 100 ms respectively.

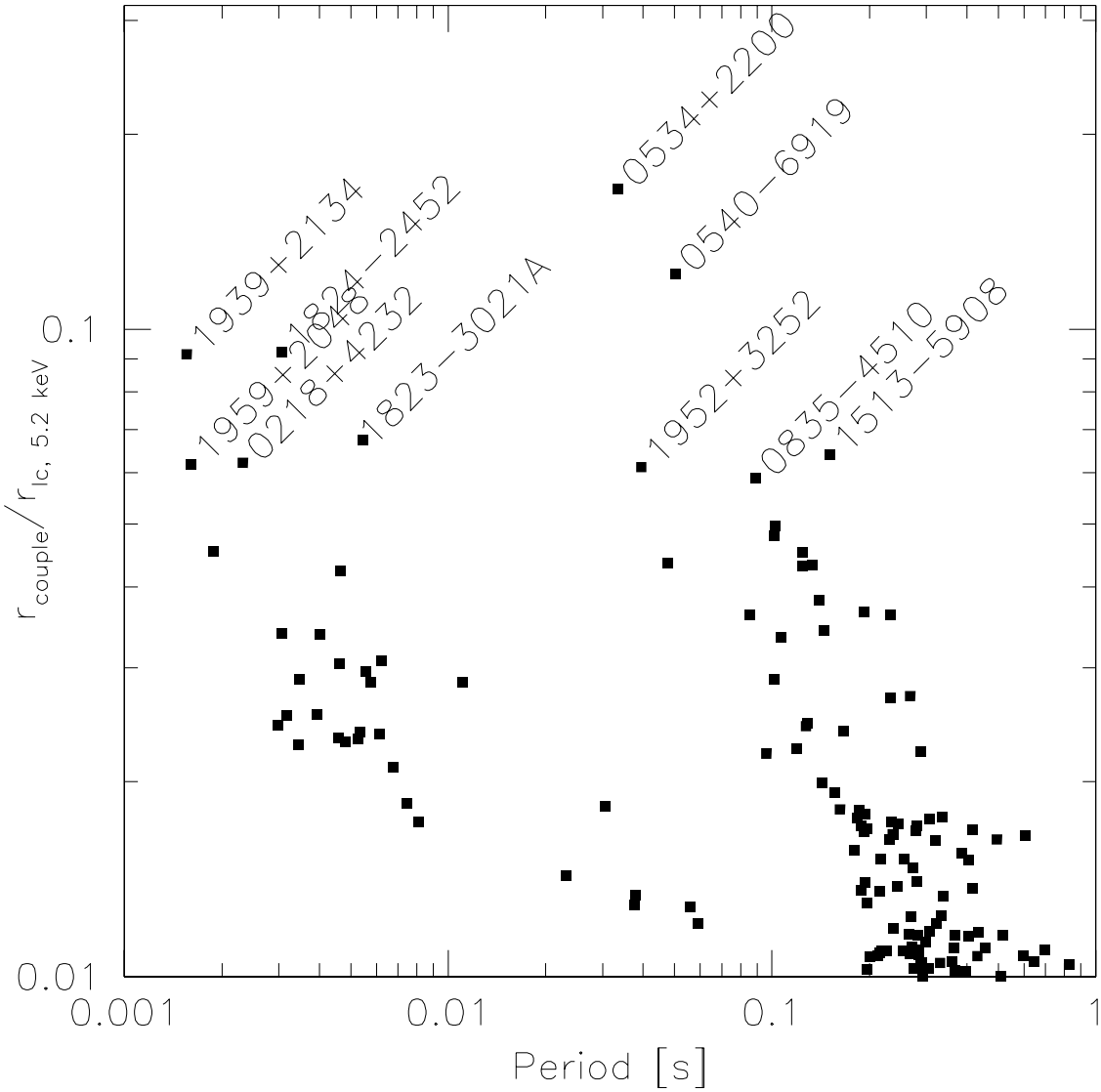

Fig. 4.— The ratio of the coupling radius at 5.2 keV to the radius of the light cylinder for the known radio pulsars. Only pulsars with $r_{\rm coupling}/r_{\rm lc} > 0.01$ are plotted.

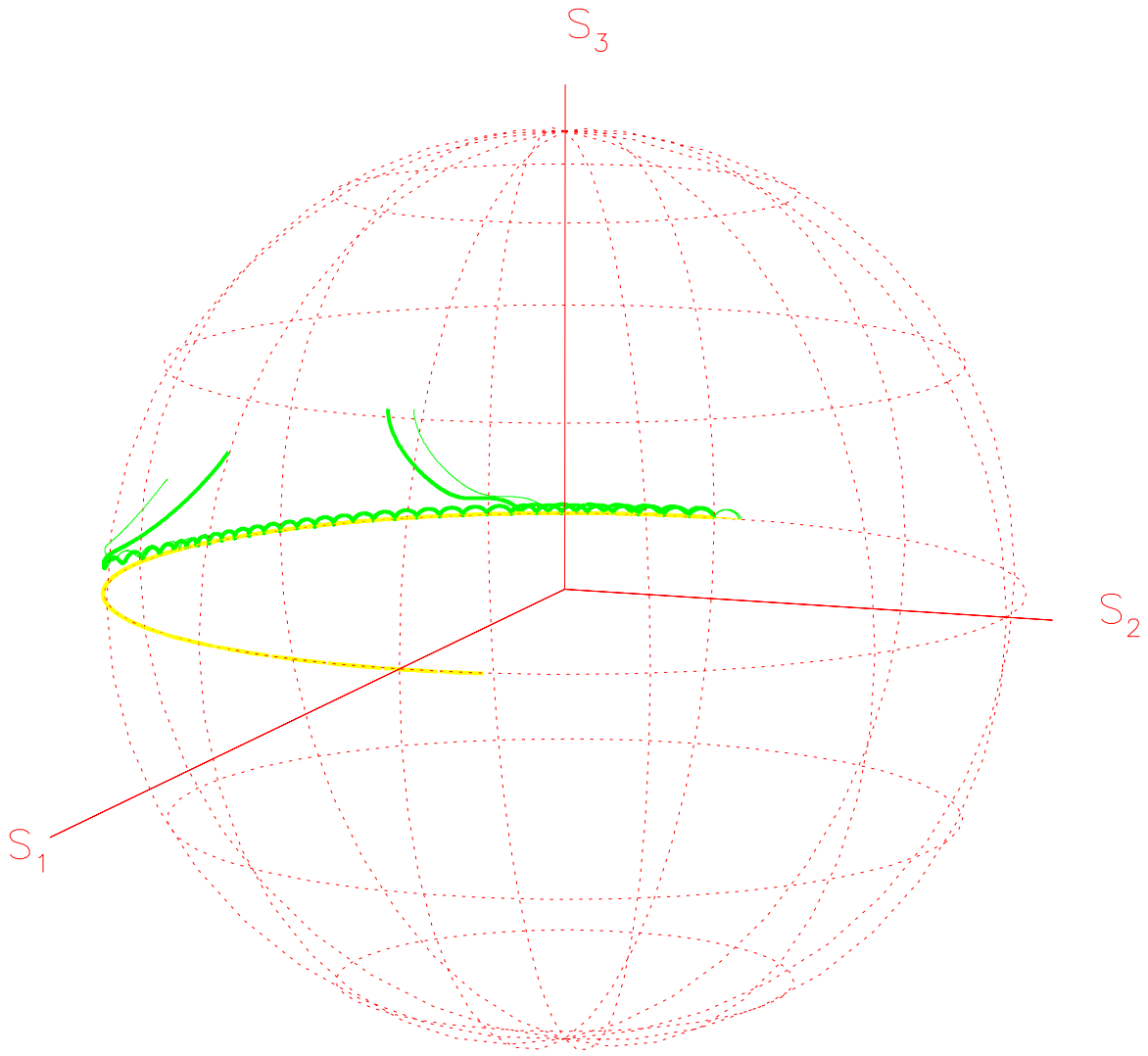

Fig. 5.— The evolution of the Stokes parameters on the Poincaré sphere for photons leaving the surface of the Crab pulsar at the moment the observer crosses the Prime Meridian. The bold lines depict the corotating dipole, and the light ones the Deutsch field. The energies plotted are 5.2 keV and 5.2 MeV. The bold line in the 1-2 plane is the birefringent vector $\hat{\mathbf{\Omega}}$. The photons' polarization vectors and the birefringent vector all start from the -1 direction. The lower energy photons follow $\hat{\mathbf{\Omega}}$ for a shorter time than do the higher energy ones. Since the mode recoupling is not instantaneous, a circular component (S_3) is generated.

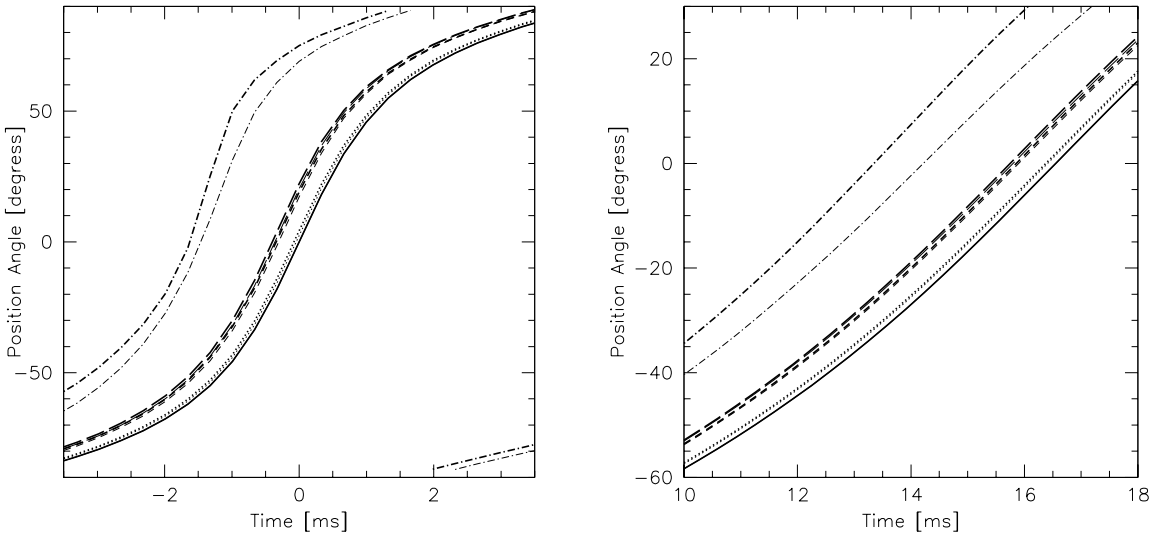

Fig. 6.— The position angle as a function of photon energy and time for our model of the Crab pulsar. From left to right, the energies are 5.2 Mev (dot-dashed), 5.2 keV (long-dashed), 2.6 keV (short-dashed), 4.48 eV (dotted) and zero energy (solid). The bold lines follow the corotating dipole model, and the light lines follow the Deutsch model.

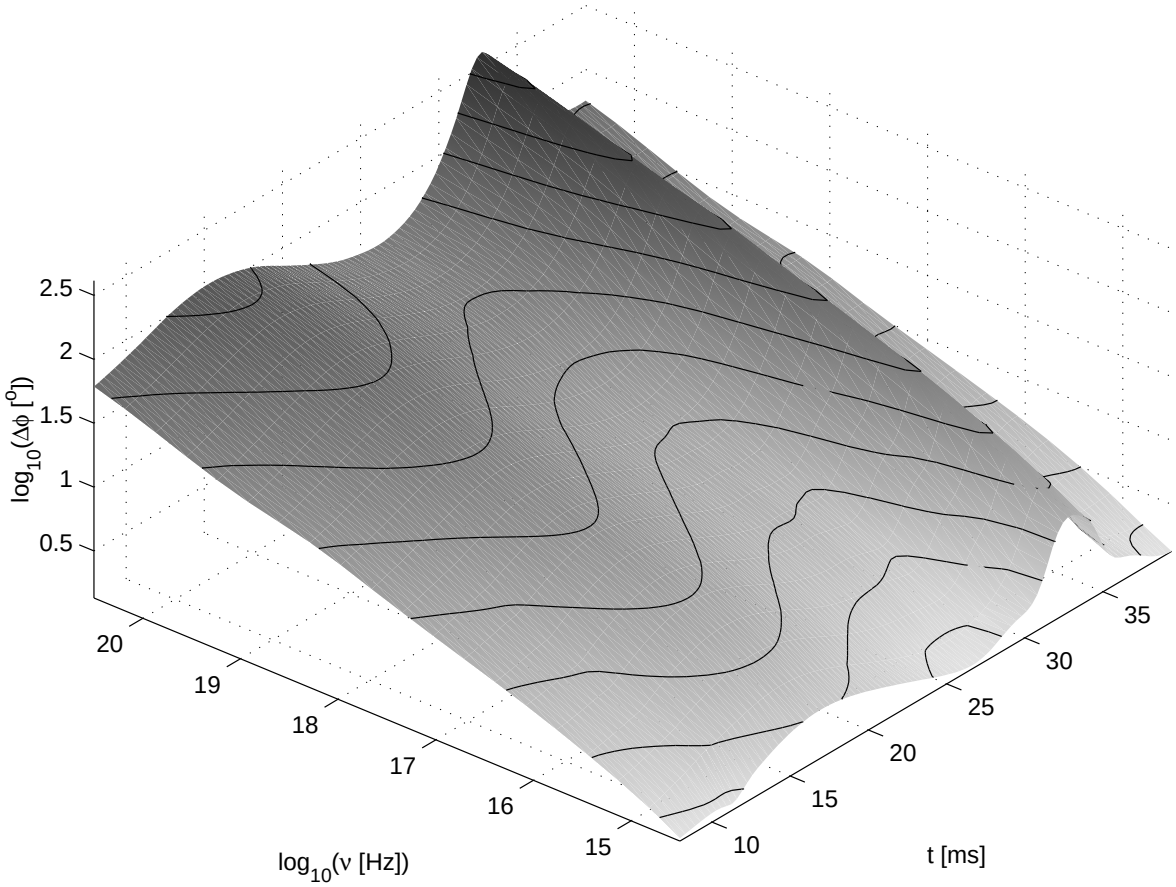

Fig. 7.— The difference between the final position angle of a photon emitted at a particular time and energy and the position angle of a zero energy photon emitted at the same time. The model is for the Crab pulsar surrounded with a Deutsch field.

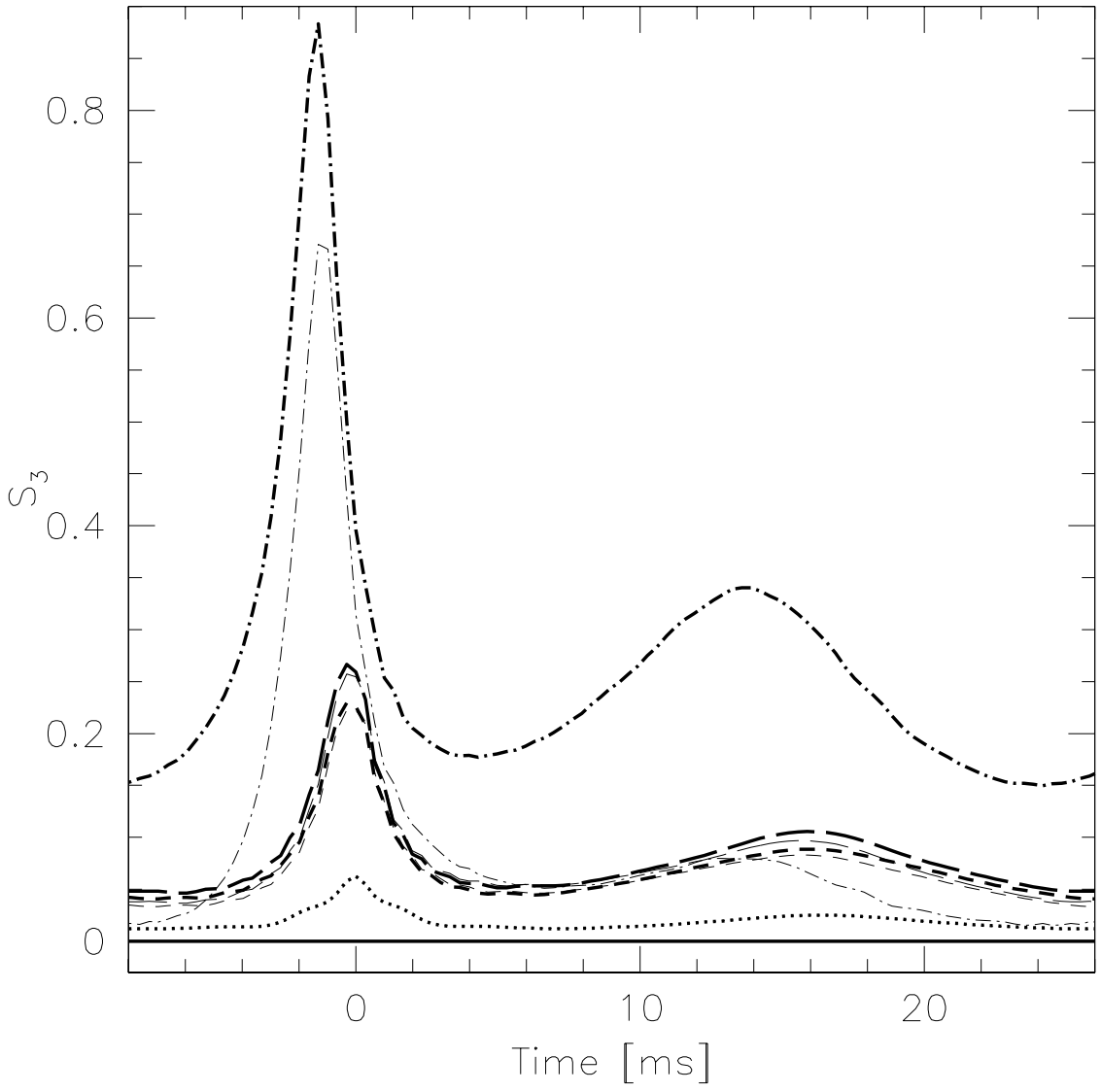

Fig. 8.— The circular component of the radiation as a function of photon energy and time for the Crab pulsar, assuming the initial polarization is complete (i.e., $|\mathbf{s}| = 1$; otherwise, it should be normalized to its smaller value). The energies are 5.2 MeV (dot-dashed), 5.2 keV (long-dashed), 2.6 keV (short-dashed), 4.48 eV (dotted) and zero energy (solid). The bold lines follow the corotating dipole model, and the light lines follow the Deutsch model.

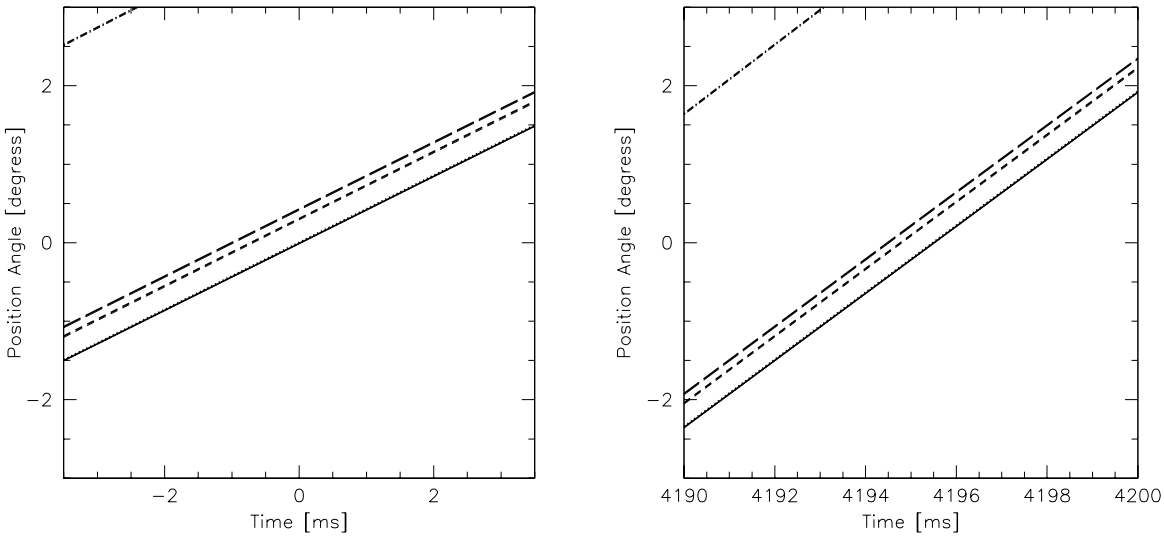

Fig. 9.— The position angle as a function of photon energy and time for our model of RXJ 0720.4-3125. We have taken $B_{0,\mathrm{equator}} = 10^{14}$ G, $\theta = 85^{\circ}$ and $\Psi = 90^{\circ}$. From left to right, the energies are 5.2 Mev, 5.2 keV, 2.6 keV, 4.48 eV and zero energy.

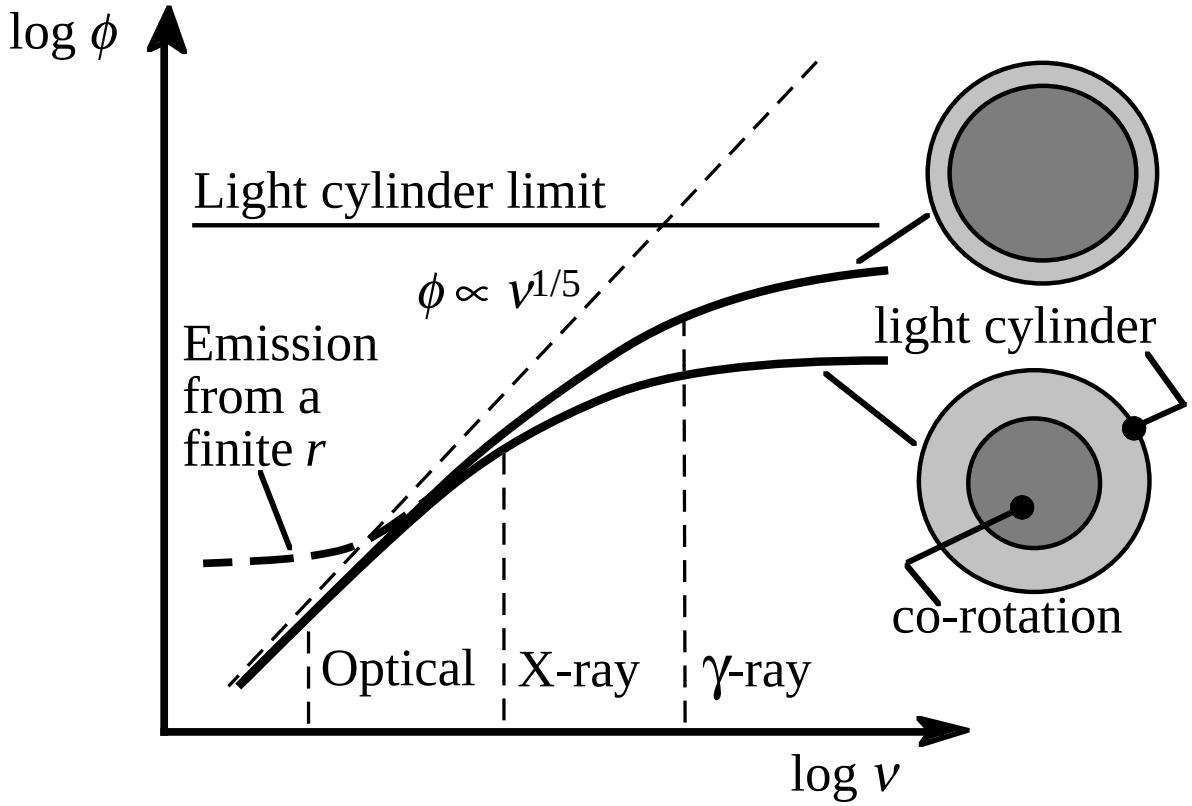

Fig. 10.— A schematic depiction of the expected phase lag at a given rotation phase of the NS. Lower frequency photons follow the changing magnetic field only over a short distance from the neutron star, and thus the modes couple when the local direction of the magnetic field has not changed much since emission. The polarization modes of higher energy photons couple further away and thus follow its changing direction further, creating a phase lead between the photon and the NS dipole direction. The magnetosphere rotates as a solid body only up to the co-rotation radius (which must be less than the radius of the light cylinder); consequently, a photon's phase lead will not be increased anymore once it begins traveling through the retarded magnetic field. If the emission process takes place at a finite radius, the lower energy photons could already be emitted outside the decoupled region. In such a case, they would suffer no phase lag.